Understanding activity trends in furfural hydrogenation on transition metal surfaces

Sihang Liu[1], Nitish Govindarajan[1,2*], Karen Chan[1]

1. Catalysis Theory Center, Department of Physics, Technical University of Denmark (DTU), 2800 Kgs. Lyngby, Denmark

2. Materials Science Division, Lawrence Livermore National Laboratory, 7000 East Avenue, Livermore, California 94550, United States

*Email: govindarajan1@llnl.gov

Abstract

Furfural hydrogenation to furfuryl alcohol is an industrially significant reaction for biomass valorization. The hydrogenation process has been mainly catalyzed by chromite-based materials that are notorious for their toxicity, thereby highlighting the need to find alternate catalyst materials. In addition, there is a gap in the mechanistic understanding of furfural hydrogenation on transition metal surfaces. Herein, we combine density functional theory calculations and microkinetic modeling to study the reaction mechanism of furfural hydrogenation to furfuryl alcohol on terrace (111/0001) and stepped (211) transition metal surfaces. We find the rate-determining steps for furfural hydrogenation to depend on the identity of the metal, where the strong binding metals are limited by desorption of the product (furfuryl alcohol) while the moderate and weak binding metals are limited by steps involving surface hydrogenation or H_2 activation. We show that the binding energy of furfural is a good descriptor to rationalize and predict the activity trends for the production of furfuryl alcohol. Among the metal and bulk/single atom alloy surfaces investigated in this work, we find Cu-based alloys to be the most active catalysts, with CuNi alloys predicted to be promising candidates for furfural hydrogenation.

Introduction

Given the depletion of fossil resources and their impact on the climate, alternatives to produce chemicals and fuels are urgently needed. The catalytic conversion of biomass serves as a promising choice in this regard[1,2]. For example, we can decompose lignocellulose, one of the most abundant biomass resources[3] (> 170 billion metric tons per year), via hydrolysis[4] into platform chemicals, such as liquid alkanes, 5-hydroxymethylfurfural (HMF), and furfural (denoted as FCHO in this work where F represents the furan ring). Furfural is a crucial bio-based molecule, with a wide range of applications in synthesizing downstream products such as pharmaceuticals and polymers[5,6]. Concurrently, the majority (> 60%) of furfural is used to produce furfuryl alcohol (FCH_2OH) via catalytic valorization[7], which is not only a key monomer for synthesizing furan resins, lysine, vitamin C and other chemicals, but also a crucial intermediate for the production of other deeply hydrogenated products such as 2-methylfuran, tetrahydrofurfural, and 2-methyltetrohydrofuran[8,9]. Furfuryl alcohol is one of the simplest products from furfural hydrogenation, with a relatively well-established reaction pathway[10,11], and can be regarded as a model reaction to understand the valorization of furfural and other biomass-derived chemicals.

Copper chromite catalysts ($CuCrO_x$) are currently used in industry to catalyze furfural hydrogenation to furfuryl alcohol with high yields (>95%) due to their ability to selectively hydrogenate C=O bonds without affecting the C=C bonds[12,13]. However, $CuCrO_x$ catalysts suffer from serious deactivation and can release toxic chromite over time to contaminate the product[14]. As a result, there is a growing interest to find more environment-friendly alternatives to replace the Cr component in $CuCrO_x$ catalysts[15]. A number of transition metals besides Cr have shown activity towards furfuryl alcohol production from furfural, e.g., Au[16], Co[17], Ir[18], Ni[19–21], Pd[22,23], Pt[24], Rh[25] and Ru[26]. Especially, Cu has been widely investigated and shown high selectivity towards furfuryl alcohol[27–31]. In addition, Cu-based alloys e.g., CuPt[32], CuPd[33] and CuNi[34] have shown 1-3 orders of magnitude higher turnover frequency (TOF) towards the production of furfuryl alcohol relative to monometallic Cu.

Over the past decade, there have been some mechanistic studies based on density functional theory (DFT) for furfural hydrogenation on transition metal surfaces. The reaction pathway towards furfuryl alcohol (cf. Scheme 1) has been proposed to occur via the hydrogenation of FCHO* (* indicates the species is adsorbed on an active site) by a surface hydrogen (H*) that is produced via the dissociation of H_2 gas (H_2 activation) to form either FCHOH* or FCH_2O*. Further hydrogenation of FCHOH*/FCH_2O* results in the formation of FCH_2OH*, which is desorbed to produce the product, furfuryl alcohol (FCH_2OH).[35,36]

Several possible rate-limiting steps have been identified in the reaction pathway shown in Scheme 1 based on the metal identity. For instance, on Cu(111), the hydrogenation of FCHO* to FCH_2O* was identified as the rate-determining step for furfuryl alcohol formation[35], while the formation of FCHOH* is suggested to be the rate-limiting step on Pd(111)[37] and Ni(111)[38] surfaces. In contrast to Ref. 37 and 38, Liu et al. identified the desorption of adsorbed furfuryl alcohol to have the highest activation barriers on both Pd and Pt surfaces[39]. We note that the differences in these studies are likely due to the use of different adsorbate configurations, the employed XC functional with/without dispersion corrections. Therefore, the reaction mechanism for furfural hydrogenation on transition metal surfaces including the pathways for H_2 activation and the nature of the rate-limiting steps are currently under debate. The adsorption energy of furfural (ΔE_{FCHO}) and metal identity dependent adsorption configurations of furfural have been used to explain furfural hydrogenation activity on different metal surfaces[36,40], indicating ΔE_{FCHO} to be potential activity descriptor for furfural hydrogenation. As the simplest furfural conversion reaction and the starting step to other value-added products, the lack of comprehensive understanding of the reaction mechanism hinders the rational catalyst design for this process and beyond.

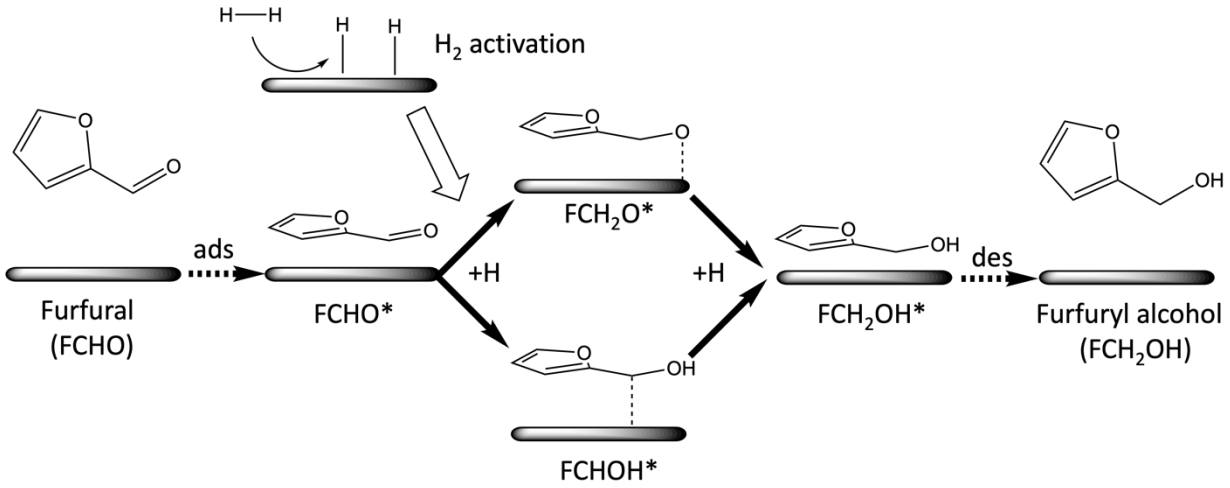

Scheme 1. Possible reaction pathways proposed for furfural hydrogenation to furfuryl alcohol on transition metal surfaces. ads and des indicate adsorption and desorption steps respectively.

Herein, we present a comprehensive mechanistic study based on DFT calculations and microkinetic simulations to identify rate-limiting steps and activity trends for furfural hydrogenation towards furfuryl alcohol on transition metal and alloy surfaces. We find the activity of the weak-binding metals (e.g., Au) to be limited by H_2 activation or hydrogenation of furfural species, while strong-binding metals (e.g., Pt) are poisoned by the adsorption of furfural. The activity volcano indicates that Cu is the most active catalyst among pure metal surfaces and the stepped surfaces of weak/moderate-binding metal surfaces are more active than terraces, while the opposite trend is observed on strong-binding metals. We show that bulk and single atom alloys could further promote the activity for furfural hydrogenation beyond monometallic surfaces. Notably, Cu-based Ni-diluted single atom alloys ($Cu@Ni_1$) and bulk Cu alloys (Cu_3Ni_1) are identified as promising candidates that can meet the requirements of high activity, less expensive and low toxicity required for the development of next-generation catalysts for furfural hydrogenation.

Computational details

Density functional theory calculations were performed using the Vienna Ab initio Software Package (VASP)[41] employing the generalized gradient approximation (GGA) using the Perdew-Burke-Ernzerhof (PBE) exchange-correlation functional [42]. Core electrons were described using

projector augmented wave (PAW) potentials[43]. The PBE calculations were supplemented with Grimme's D3[44] correction to account for dispersion interactions of the furan ring with the metal surfaces. Note that PBE-D3 functional was suggested to overbind furanic molecules, but the trends are not affected on different metal surfaces[39]. The Atomic Simulation Environment (ASE)[45] was used to build 4 × 4 × 4 (111) or (0001) slabs and 3 × 4 × 4 (211) slabs that represent terrace and stepped surfaces, respectively. The bottom two layers of surface were fixed at their bulk interatomic distances. A dense Monkhorst–Pack[46] k-point mesh of 12 × 12 × 12 was used to obtain the optimized lattice constants of the metal, while k-point meshes of 3 × 3 × 1 and 4 × 3 × 1 were used to sample the reciprocal first Brillouin zone for the (111)/(0001) and (211) metal slabs respectively. A 15 Å vacuum spacing is added in the z direction for all the supercells. A plane-wave cutoff of 400 eV was used in the geometry optimizations. The geometry optimizations were considered converged when the maximum residual force on each atom was less than 0.02 eV/Å. The reaction barriers for furfural hydrogenation reaction on (111) surfaces were calculated by using the climbing image nudged elastic band (CI-NEB)[47] and optimized by dimer[48] methods, with a force convergence criterion of 0.05 eV/Å on each atom. The transition states were confirmed by examining that only one large single imaginary frequency exists. The microkinetic simulations were performed using the open source CatMAP code[49] based on the mean-field approach and the steady-state approximation including a self-consistent description of adsorbate−adsorbate interactions. In the microkinetic model, the binding energies of FCHO* and H* (ΔE_{FCHO} and ΔE_H) were used as descriptors and the calculated energetics on (111) surfaces were used as input for the scaling relations and the activity volcano shown in Figure 3b and 4b, respectively. The results for the stepped surfaces (211) and bulk/single atom alloys were then fitted to the activity volcano plot shown in Figure 4b. Further details of the microkinetic simulations are provided in the Supporting Information.

Results and discussion

The proposed reaction mechanism for furfural hydrogenation towards furfuryl alcohol is shown in Scheme 1. Overall, the bare metal surface catalyzes both furfural hydrogenation reaction and

H_2 activation. The adsorbed H* is the hydrogen source for gas-phase furfural hydrogenation reactions. For all the metals considered in this work, we have performed simulations on (111)/(0001) and (211) surfaces that are representative of terrace and step sites respectively.

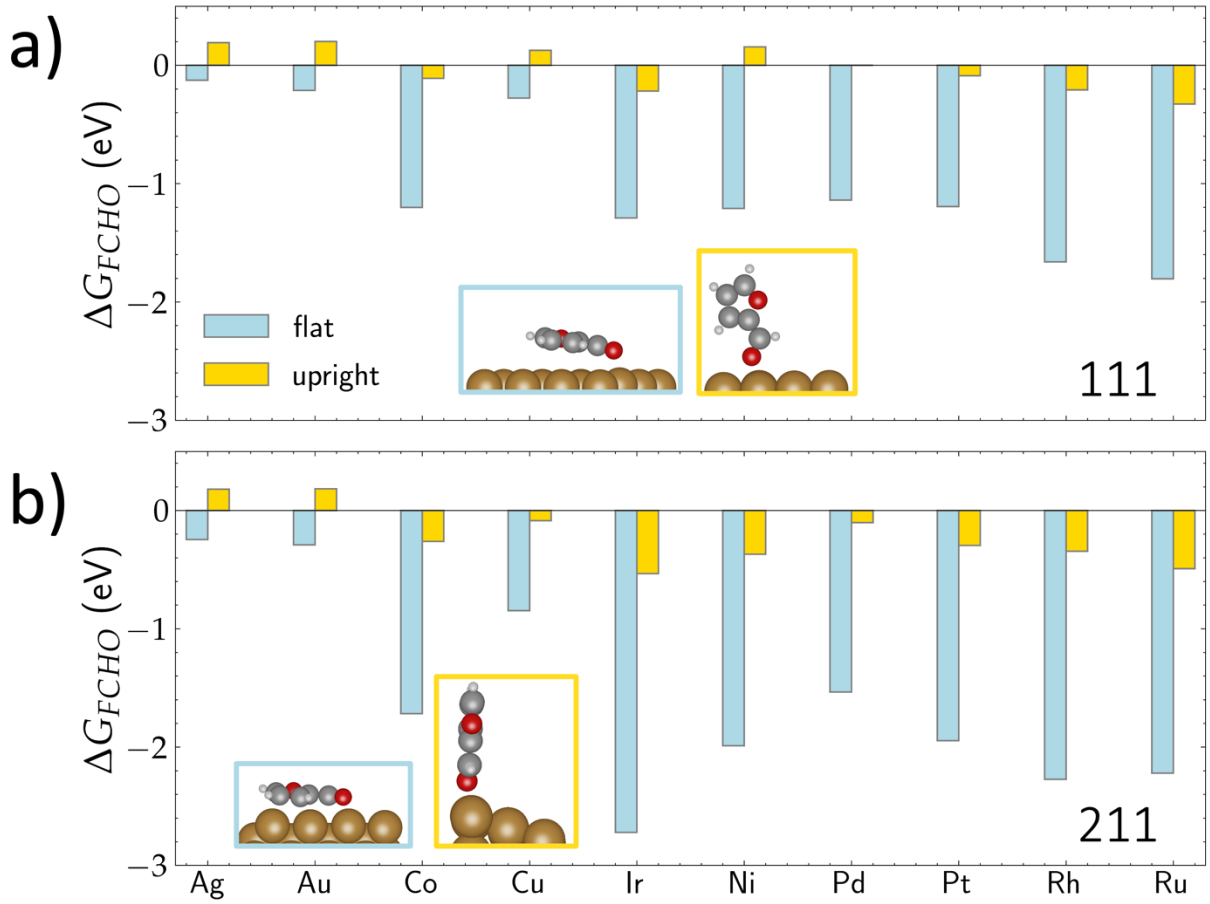

Figure 1. Adsorption free energies of furfural (FCHO) with flat or upright configurations on a) 111 and b) 211 metal surfaces. Simulation conditions: 400K, P_{FCHO} = 0.1bar. The representative adsorption configurations of FCHO on Cu surfaces are shown as insets.

As shown in Figure 1, flat adsorption configurations of furfural are more stable than upright ones on all the studied metal surfaces (including terrace and step sites) under hydrogenation reaction conditions, in agreement with previous theoretical studies[10,36,38,50]. The interaction of the metal surface with both the furan ring (F) and aldehyde group (CHO) is likely the reason for the preference of flat configurations over the upright ones, with the latter only interacting with the

surface via the aldehyde group. Moreover, the stronger the adsorption of furfural (i.e., more negative ΔG_{FCHO}), the larger the difference in adsorption energies of two configurations. Our calculations suggest that at low coverages, the flat adsorption configuration of FCHO* might dominate on the metal surfaces investigated in this work, which is in line with direct scanning tunneling microscopy studies that sub-monolayer of furfural adsorbs in a flat configuration on Pt(111)[51].

At higher coverages (ca. 0.5 ML), furfural is theoretically predicted to prefer tilted or upright configurations on Pd(111) in order to minimize the effects of lateral interactions[52]. We also find that on Cu, Pd and Pt(111) surfaces, furfural prefers to take a flat adsorption configuration at low coverages, and a tilted configuration at 0.25 ML and an upright configuration at coverages >0.33ML (cf. Figure S1). However, previous temperature-programmed studies of furfural desorption on Pd(111)[50] and Pt(111)[53] suggest that at reaction temperatures typically applied for gas-phase furfural hydrogenation (400-500 K), the less stable adsorption configurations, e.g., upright, tend to desorb due to lower binding strength relative to flat configurations. Besides, the typical tilted configuration of furfural[52] still binds the surface with the -CHO group and only tilts the furan ring away, which is not involved in the reaction pathway for furfuryl alcohol. As a result, we assume that furfural and all the other reaction intermediates take the flat configuration on all the considered surfaces in the calculation of reaction energetics discussed below.

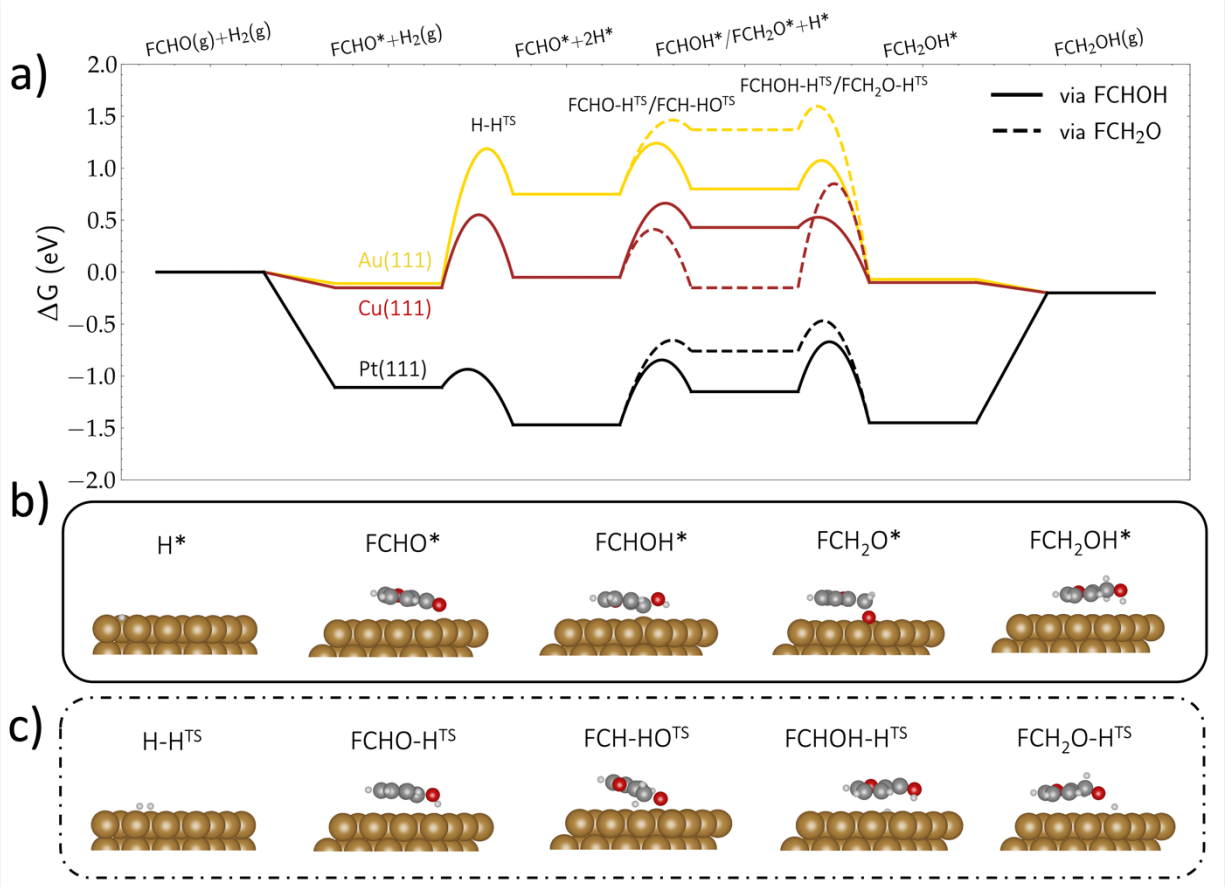

Figure 2. Free energy profiles for furfural hydrogenation on Au(111), Cu(111) and Pt(111) surfaces via FCHOH* (solid lines) and FCH_2O* (dotted lines) at 400k, P_{FCHO} = 0.1bar, P_{H2} = 1bar; b) The adsorption configuration of stable intermediates, and c) the transition state structures on Cu(111).

The free energy diagrams for furfural hydrogenation to furfuryl alcohol at 400 K on three representative surfaces: Au(111), Cu(111) and Pt(111) are shown in Figure 2a. The two possible pathways towards furfuryl alcohol via FCHOH* and FCH_2O* are shown in solid and dashed lines respectively. Given the similarity in adsorption configurations of the reaction intermediates on different metal surfaces, we only depict adsorption configurations of the stable reaction intermediates and transition states on Cu(111) in Figure 2b,c. The configurations of all the reaction intermediates and transition states for the other surfaces investigated in this work are provided in database link shown below.

We highlight the following observations based on the free energy diagram for furfural hydrogenation on Au, Cu and Pt (111) surfaces shown in Figure 2a:

1. H_2 activation is rate-determining step (RDS) for furfural hydrogenation on Au(111) as a result of its high activation barrier (ca. 1.21 eV), while being facile on Pt(111) and Cu(111) surfaces.
2. The hydrogenation of FCH_2O* with an activation barrier of 0.98 eV is the RDS on Cu(111) in line with a previous theoretical study[35]. In contrast, we find the hydrogenation of furfural via the FCHOH* intermediate to be facile on Pt(111) and Au(111) surfaces. Previously, Sitthisa et al. showed that the formations of FCHOH* and FCH_2O* are both endothermic on Cu(111) surface[11]. However, we find that FCH_2O* formation is exothermic and thermodynamically more favored by ca. 0.54 eV than the formation of FCHOH* on Cu(111) as shown in Figure 2a. The discrepancy between our observations and those by Sitthisa et al. could be due to the differences in the configuration of FCH_2O* - we find the adsorption energy of the "flat" configuration (cf. Figure S1) reported in their work to be less stable by ca. 0.42 eV than the "bending" configuration where the O of the -CH_2O group in FCH_2O* inserts in the hollow site on Cu(111) as shown in in Figure 2b.
3. Finally, we find that the desorption of the product (FCH_2OH*) limits the hydrogenation activity on Pt(111), due to its strong binding of furfural species. In fact, furan and other ring-opening hydrocarbons were reported to be side-products on Pt[51], Ru[54] and Ni[55] catalysts at high temperatures. It is likely that the strong adsorption of furfural on these metal surfaces hinders further hydrogenation by reducing relative H* coverage on the surface and triggers C-C bond breaking and ring-opening reactions at high temperatures.

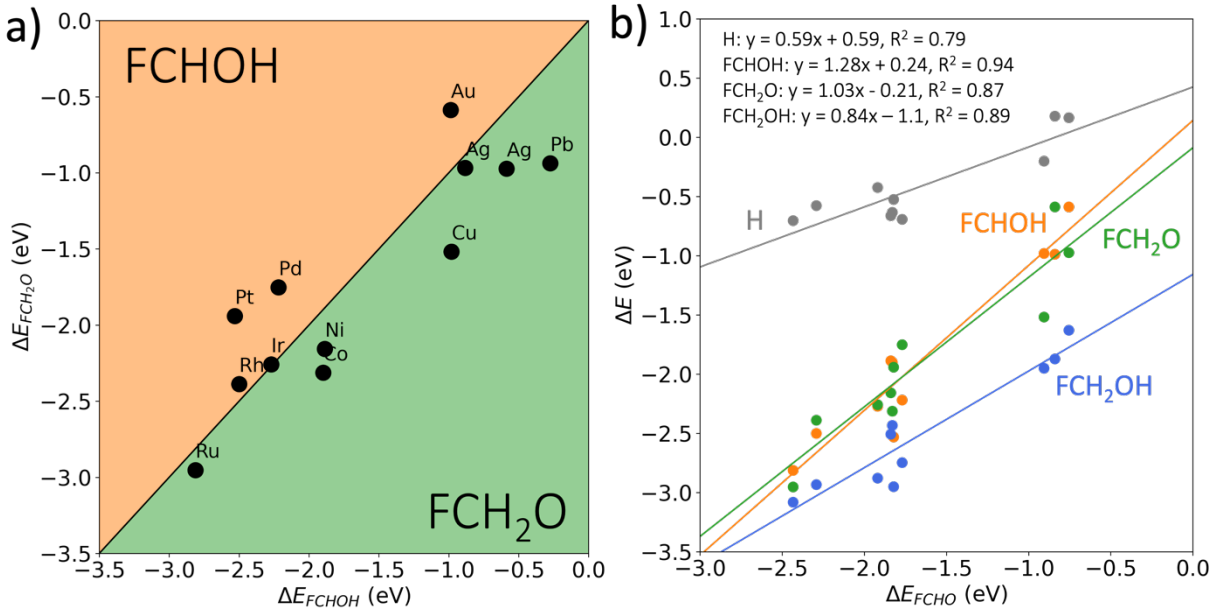

Figure 3. a) The adsorption energies of FCHOH and FCH_2O on the different metal (111) surfaces investigated in this work. The orange and green areas represent FCHOH-favored and FCH_2O-favored regions respectively; b) Scaling relationships of adsorption energies between FCHO and the other stable adsorbates involved in the reaction pathway for furfural hydrogenation.

We further observe a metal identity dependent preference for the two key intermediates on (111) surfaces, i.e., FCHOH* and FCH_2O* as shown in Figure 3a. Generally, FCHOH* is more stable than FCH_2O* on Au, Pt, Pd and Rh surfaces, where both the aldehyde group and furan ring of FCHOH* interact with the metal surface except for a weak-binding metal like Au where only the aldehyde group interacts with the metal surface, as shown in Figure S3. In contrast, the oxyphilic surfaces (surfaces with a higher tendency to form metal oxides) including Ag, Ni, Cu, Co, Pb and Ru, favor the formation of FCH_2O* over FCHOH*. Notably, the adsorption configuration of FCH_2O* on these oxyphilic surfaces with O atom buried at the hollow site as shown in Figure S4, might hinder further hydrogenation of FCH_2O* as is observed for the Cu(111) surface (*vide supra*). A similar preference of adsorbates based on carbon-philic and oxygen-philic metals was reported in a recent study to govern the reaction pathway and selectivity during glycerol dehydrogenation.[56]

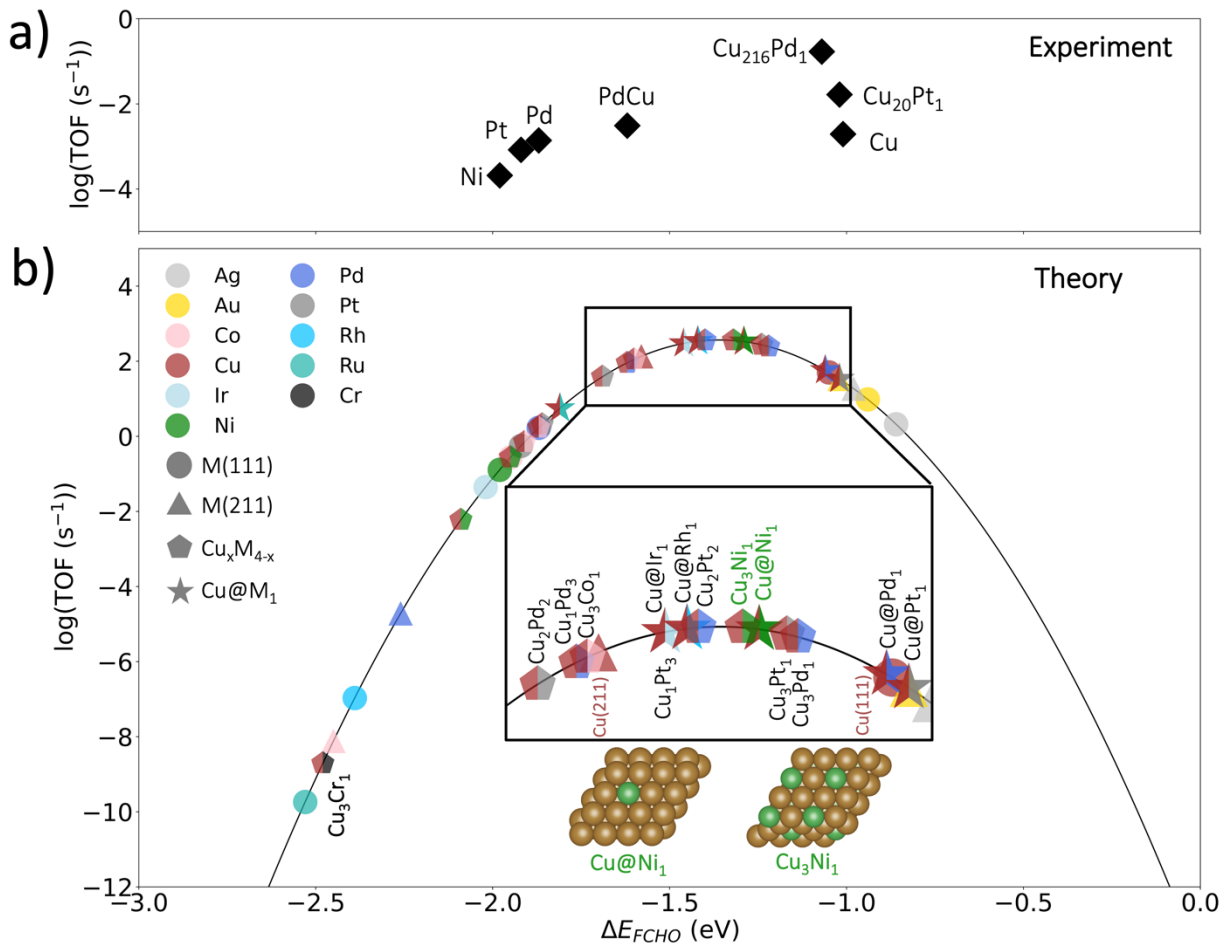

Figure 4. Activity volcano for furfural hydrogenation towards furfuryl alcohol. a) The adapted TOF plot from experiments for Cu[57], Ni[58], Pd[59], Pt[60], PdCu[59], $Cu_{216}Pd_1$[59], and $Cu_{20}Pt_1$[60]. Note that the ΔE_{FCHO} on the x-axis corresponds to the (111) surface of the respective metal. b) The simulated TOF plot based on microkinetic simulations at 400K, P_{FCHO} = 1bar and P_{H2} = 1bar. M represents a metal surface and Cu_xM_{4-x} and $Cu@M_1$ represent Cu-based bulk alloys and single-atom alloys with M, respectively. Representative configurations of Cu_3Ni_1 and $Cu@Ni_1$ surfaces are shown as insets.

Based on the reaction energetics reported in Figure 2 and scaling relationships in Figure 3b, we further develop a mean-field microkinetic model including explicit adsorbate-adsorbate interactions using the CatMAP code[49] to study the activity for furfuryl alcohol production over different metal surfaces under reaction conditions. The considered elementary steps and other simulation parameters are discussed in the **Microkinetic Simulation** section in the **Supporting Information**. We find that the binding energies of all reaction intermediates involved in furfural

hydrogenation to scale well with FCHO* (cf. Figure 3b), indicating that we could use a single activity descriptor, *i.e.*, the adsorption strength of furfural ΔE_{FCHO}. The activity trends of both experiment and theory are shown in Figure 4.

Cu is theoretically predicted to be the most active catalyst for furfural hydrogenation towards furfuryl alcohol (cf. Figure 4b) among all the elemental transition metals considered in this work. The high TOF of Cu results from a moderate barrier for H_2 activation (cf. Figure 4) and suitable adsorption strength of furfural species, which lead to a good overall activity.

Stepped surfaces promote the activity on weak-binding metals, while they suppress the activity on strong-binding metals. As can be seen in Figure 4b, Cu(211) is predicted to have a higher activity by ca. 1 order than Cu(111) for furfural hydrogenation, indicating that the introduction of under-coordinated sites on Cu surfaces might lead to increase in the activity for furfuryl alcohol production. A similar trend is observed on weak-binding surfaces including Ag and Au with the stepped (211) surfaces predicted to have higher activity than (111) surfaces. On the strong-binding leg of the activity volcano plot in Figure 4b, Pd(111) is predicted to be the most active monometallic surface, followed by Co(0001) and Ni(111). In contrast to weak-binding metals, for the strong-binding metals, stepped surfaces (211) are predicted to have lower activity than the (111) surfaces. As shown in Figure 1, stepped surfaces exhibit stronger binding of furfural (i.e., more negative ΔG_{FCHO}) especially for strong-binding metals compared to their (111) counterparts, while the H* adsorption is a lot less sensitive to the facet identity (cf. Figure S5). As a result, the H* coverages on strong-binding stepped surfaces are reduced as shown in Figure S5, while the FCHO* coverages only increase moderately due to large adsorbate-adsorbate interactions. Consequently, the second-order dependence of hydrogenation activity on H* coverage and first-order dependence on FCHO* coverage lead to an overall decreased activity towards furfuryl alcohol formation on the strong-binding surfaces (i.e., Pt, Pd, Ir, Ni, Co, Rh and Ru).

The simulated activity volcano (for monometallic surfaces) in Figure 4b suggests that there remains space for improvement in activity, which can also be seen in the experimental TOF data that was obtained at similar reaction conditions in Figure 4a.[59] In order to identify catalyst materials that might be closer to the top of the activity volcano in Figure 4b, we studied bulk alloys and single atom alloys (SAAs) by combining one metal on the weak-binding leg, i.e., Cu and one metal on the strong-binding leg, e.g., Pt, Pd and Ni. For the convenience of direct synthesis in experiments, we only considered alloy candidates which have been reported in previous experimental studies of C=O hydrogenation reactions performed under similar reaction conditions (temperature and pressure)[61–65]. We find that CuCr alloy binds furfural too strongly even with a dilute Cr component (i.e., Cu_3Cr_1), leading to a relatively low activity. Note that the CuCr might be oxidized during the reaction, therefore the theoretical CuCr alloy model here might not be the actual active surfaces. Several Cu based alloys that were investigated are predicted to have high activity (close to the top of the activity volcano) as can be seen in the inset in Figure 4b. CuPd, CuPt, CuCo and CuNi bulk alloys and Ir, Rh, Ni, Pd, Pt-doped Cu single atom alloys show improved activity for furfural hydrogenation compared to their parent metals. This observation is in line with the experimental observations in Figure 4a: $Cu_{216}Pd_1$ single atom alloy in Ref[59] shows over two orders of magnitude higher TOF towards furfuryl alcohol than Cu and Pd on Al_2O_3 support; dilute CuPt alloys in Ref[60] are predicted to have more than one order of magnitude higher TOF compared to pure Cu and Pt catalyst. However, these alloy candidates have the disadvantage that they still contain expensive noble metals (Pt, Pd).

Interestingly, Cu-rich Cu_3Ni_1 and $Cu@Ni_1$ surfaces are predicted to have high activity for the production of furfuryl alcohol, while CuNi alloys with high Ni content including Cu_2Ni_2 and Cu_1Ni_3 are predicted to have low activity (cf. Figure 4b) due to the over-binding of furfural on the Ni-rich active sites. The prediction that Cu rich CuNi alloys have high activity for furfural hydrogenation is in agreement with a recent study by Weerachawanasak et al. where CuNi alloys with a Cu-rich component were reported to show higher yields for furfuryl alcohol production relative to pure Cu and Ni-rich catalysts.[58] In addition, Ni-rich catalysts are reported to display activity towards further hydrogenated products in vapor phase, e.g., tetrahydrofurfuryl alcohol (THFA)[66].

Therefore, diluting Ni content in Cu catalyst is crucial to obtain high selectivity and activity towards furfuryl alcohol. Considering the abundance, noble-metal-free and low toxicity of both copper and nickel, we advocate for future research efforts to extensively study CuNi based bimetallic catalysts for furfural hydrogenation as they can help resolving some of the major issues that currently plague the industrial production of furfuryl alcohol using chromite-based catalyst materials.

Before closing the discussion, we highlight the following limitations of our study. First, we focused on the simplest furfural valorization reaction involving the conversion of furfural to furfuryl alcohol and ignored possible side reactions, e.g., ring-opening and further hydrogenation, which might selectively occur under harsher reaction conditions (i.e., higher temperature and pressure or in the presence of specific solvents)[15]. As a result, our work does not provide insights on the selectivity of furfural hydrogenation but only indicates the activity trends of furfural hydrogenation on metal surfaces. Furthermore, our model does not explicitly consider the effects of the oxide support typically used in experiments, which could potentially impact the reactivity of furfural hydrogenation reactions as shown in previous studies[16,27,67,68]. Finally, we did not consider possible surface reconstruction, segregation and oxidation under *operando* conditions, which might introduce discrepancies in the observed structure-activity relationships[69–71].

Conclusions

To summarize, we have performed DFT calculations and microkinetic modeling to study the activity trends in furfural hydrogenation to furfuryl alcohol on metal surfaces. The rate-determining steps were identified to be H_2 activation, surface hydrogenation of FCHOH*/FCH_2O* and furfural desorption on weak, moderate and strong-binding surfaces as represented by Au(111), Cu(111) and Pt(111) surfaces respectively. We show that the furfural adsorption energy can serve as an effective activity descriptor for furfural hydrogenation, where the moderate binding strength of furfural leads to maximal predicted activity. The microkinetic simulations show that stepped (211) surfaces are more active than terrace (111) surfaces for moderate/weak binding metals including Cu, Ag and Au, while the opposite trend is observed on the strong-

binding metals including Pt, Pd, Ir, Ni, Co, Rh and Ru. These observations highlight facet-dependent catalyst design principles. We further predict several Cu-based alloys to display high activity towards furfuryl alcohol production beyond monometallic candidates. In particular, we find that CuNi alloys with dilute Ni component are promising candidates to replace Cr-containing catalysts currently employed in the industrial hydrogenation of furfural to furfuryl alcohol.

Acknowledgements

This work was supported by a research grant (29450) from VILLUM FONDEN. Writing of the manuscript by N. G was performed under the auspices of the US Department of Energy by Lawrence Livermore National Laboratory (LLNL) under Contract DE-AC52-07NA27344. We are grateful to Prof. Jens K Nørskov for his valuable comments on the manuscript.

Author Contributions

Conceptualization, S.L., N.G., and K.C.; methodology, S.L., N.G., and K.C.; software, S.L.; investigation, S.L., and N.G.; resources, K.C.; data curation, S.L.; writing original draft, S.L. and N.G.; writing review & editing, S.L., N.G., and K.C.; visualization, S.L.; supervision, K.C. and N.G.; project administration, K.C.; funding acquisition, K.C.

Notes

The authors declare no competing financial interest.

The atomic coordinates of the reaction intermediates on different metal surfaces investigated in this work, the input files for the microkinetic simulations and the scripts used to reproduce the figures in the manuscript are available at the following weblink: https://github.com/CatTheoryDTU/furfural_hydrogenation

References:

(1) Lin, L.; Han, X.; Han, B.; Yang, S. Emerging Heterogeneous Catalysts for Biomass Conversion: Studies of the Reaction Mechanism. *Chem. Soc. Rev.* **2021**, 10.1039.D1CS00039J. https://doi.org/10.1039/D1CS00039J.

(2) Huber, G. W.; Iborra, S.; Corma, A. Synthesis of Transportation Fuels from Biomass: Chemistry, Catalysts, and Engineering. *Chem. Rev.* **2006**, *106* (9), 4044–4098. https://doi.org/10.1021/cr068360d.

(3) Feng, Y.; Long, S.; Tang, X.; Sun, Y.; Luque, R.; Zeng, X.; Lin, L. Earth-Abundant 3d-Transition-Metal Catalysts for Lignocellulosic Biomass Conversion. *Chemical Society Reviews* **2021**, *50* (10), 6042–6093.

(4) Delbecq, F.; Wang, Y.; Muralidhara, A.; El Ouardi, K.; Marlair, G.; Len, C. Hydrolysis of Hemicellulose and Derivatives—A Review of Recent Advances in the Production of Furfural. *Frontiers in chemistry* **2018**, *6*, 146.

(5) Xu, C.; Paone, E.; Rodríguez-Padrón, D.; Luque, R.; Mauriello, F. Recent Catalytic Routes for the Preparation and the Upgrading of Biomass Derived Furfural and 5-Hydroxymethylfurfural. *Chem. Soc. Rev.* **2020**, *49* (13), 4273–4306. https://doi.org/10.1039/D0CS00041H.

(6) Dalvand, K.; Rubin, J.; Gunukula, S.; Wheeler, M. C.; Hunt, G. Economics of Biofuels: Market Potential of Furfural and Its Derivatives. *Biomass and Bioenergy* **2018**, *115*, 56–63.

(7) Mandalika, A.; Qin, L.; Sato, T. K.; Runge, T. Integrated Biorefinery Model Based on Production of Furans Using Open-Ended High Yield Processes. *Green Chemistry* **2014**, *16* (5), 2480–2489.

(8) Li, X.; Jia, P.; Wang, T. Furfural: A Promising Platform Compound for Sustainable Production of C_4 and C_5 Chemicals. *ACS Catal.* **2016**, *6* (11), 7621–7640. https://doi.org/10.1021/acscatal.6b01838.

(9) Mariscal, R.; Maireles-Torres, P.; Ojeda, M.; Sádaba, I.; López Granados, M. Furfural: A Renewable and Versatile Platform Molecule for the Synthesis of Chemicals and Fuels. *Energy Environ. Sci.* **2016**, *9* (4), 1144–1189. https://doi.org/10.1039/C5EE02666K.

(10) Vorotnikov, V.; Mpourmpakis, G.; Vlachos, D. G. DFT Study of Furfural Conversion to Furan, Furfuryl Alcohol, and 2-Methylfuran on Pd(111). *ACS Catal.* **2012**, *2* (12), 2496–2504. https://doi.org/10.1021/cs300395a.

(11) Sitthisa, S.; Sooknoi, T.; Ma, Y.; Balbuena, P. B.; Resasco, D. E. Kinetics and Mechanism of Hydrogenation of Furfural on Cu/SiO2 Catalysts. *Journal of Catalysis* **2011**, *277* (1), 1–13. https://doi.org/10.1016/j.jcat.2010.10.005.

(12) Adkins, H.; Connor, R. The Catalytic Hydrogenation of Organic Compounds over Copper Chromite. *Journal of the American Chemical Society* **1931**, *53* (3), 1091–1095.

(13) Rao, R.; Dandekar, A.; Baker, R.; Vannice, M. Properties of Copper Chromite Catalysts in Hydrogenation Reactions. *Journal of Catalysis* **1997**, *171* (2), 406–419.

(14) Liu, D.; Zemlyanov, D.; Wu, T.; Lobo-Lapidus, R. J.; Dumesic, J. A.; Miller, J. T.; Marshall, C. L. Deactivation Mechanistic Studies of Copper Chromite Catalyst for Selective Hydrogenation of 2-Furfuraldehyde. *Journal of catalysis* **2013**, *299*, 336–345.

(15) Wang, Y.; Zhao, D.; Rodríguez-Padrón, D.; Len, C. Recent Advances in Catalytic Hydrogenation of Furfural. *Catalysts* **2019**, *9* (10), 796. https://doi.org/10.3390/catal9100796.

(16) Li, M.; Collado, L.; Cárdenas-Lizana, F.; Keane, M. A. Role of Support Oxygen Vacancies in the Gas Phase Hydrogenation of Furfural over Gold. *Catal Lett* **2018**, *148* (1), 90–96. https://doi.org/10.1007/s10562-017-2228-9.

(17) Audemar, M.; Ciotonea, C.; De Oliveira Vigier, K.; Royer, S.; Ungureanu, A.; Dragoi, B.; Dumitriu, E.; Jérôme, F. Selective Hydrogenation of Furfural to Furfuryl Alcohol in the Presence of a Recyclable Cobalt/SBA-15 Catalyst. *ChemSusChem* **2015**, *8* (11), 1885–1891.

(18) Date, N. S.; Hengne, A. M.; Huang, K.-W.; Chikate, R. C.; Rode, C. V. Single Pot Selective Hydrogenation of Furfural to 2-Methylfuran over Carbon Supported Iridium Catalysts. *Green Chemistry* **2018**, *20* (9), 2027–2037.

(19) Banerjee, A.; Mushrif, S. H. Investigating Reaction Mechanisms for Furfural Hydrodeoxygenation on Ni and the Effect of Boron Doping on the Activity and Selectivity of the Catalyst. *J. Phys. Chem. C* **2018**, *122* (32), 18383–18394. https://doi.org/10.1021/acs.jpcc.8b01301.
(20) Nakagawa, Y.; Nakazawa, H.; Watanabe, H.; Tomishige, K. Total Hydrogenation of Furfural over a Silica-Supported Nickel Catalyst Prepared by the Reduction of a Nickel Nitrate Precursor. *ChemCatChem* **2012**, *4* (11), 1791–1797. https://doi.org/10.1002/cctc.201200218.
(21) Meng, X.; Yang, Y.; Chen, L.; Xu, M.; Zhang, X.; Wei, M. A Control over Hydrogenation Selectivity of Furfural via Tuning Exposed Facet of Ni Catalysts. *ACS Catal.* **2019**, *9* (5), 4226–4235. https://doi.org/10.1021/acscatal.9b00238.
(22) Bhogeswararao, S.; Srinivas, D. Catalytic Conversion of Furfural to Industrial Chemicals over Supported Pt and Pd Catalysts. *Journal of Catalysis* **2015**, *327*, 65–77. https://doi.org/10.1016/j.jcat.2015.04.018.
(23) Pang, S. H.; Schoenbaum, C. A.; Schwartz, D. K.; Medlin, J. W. Effects of Thiol Modifiers on the Kinetics of Furfural Hydrogenation over Pd Catalysts. *ACS Catal.* **2014**, *4* (9), 3123–3131. https://doi.org/10.1021/cs500598y.
(24) Ouyang, W.; Yepez, A.; Romero, A. A.; Luque, R. Towards Industrial Furfural Conversion: Selectivity and Stability of Palladium and Platinum Catalysts under Continuous Flow Regime. *Catalysis Today* **2018**, *308*, 32–37. https://doi.org/10.1016/j.cattod.2017.07.011.
(25) Castelbou, J. L.; Szeto, K.; Barakat, W.; Merle, N.; Godard, C.; Taoufik, M.; Claver, C. A New Approach for the Preparation of Well-Defined Rh and Pt Nanoparticles Stabilized by Phosphine-Functionalized Silica for Selective Hydrogenation Reactions. *Chemical Communications* **2017**, *53* (22), 3261–3264.
(26) Musci, J. J.; Merlo, A. B.; Casella, M. L. Aqueous Phase Hydrogenation of Furfural Using Carbon-Supported Ru and RuSn Catalysts. *Catalysis Today* **2017**, *296*, 43–50.
(27) Jiménez-Gómez, C. P.; Cecilia, J. A.; Márquez-Rodríguez, I.; Moreno-Tost, R.; Santamaría-González, J.; Mérida-Robles, J.; Maireles-Torres, P. Gas-Phase Hydrogenation of Furfural over Cu/CeO 2 Catalysts. *Catalysis Today* **2017**, *279*, 327–338. https://doi.org/10.1016/j.cattod.2016.02.014.
(28) Jiménez-Gómez, C. P.; Cecilia, J. A.; Durán-Martín, D.; Moreno-Tost, R.; Santamaría-González, J.; Mérida-Robles, J.; Mariscal, R.; Maireles-Torres, P. Gas-Phase Hydrogenation of Furfural to Furfuryl Alcohol over Cu/ZnO Catalysts. *Journal of Catalysis* **2016**, *336*, 107–115. https://doi.org/10.1016/j.jcat.2016.01.012.
(29) Jiménez-Gómez, C. P.; Cecilia, J. A.; García-Sancho, C.; Moreno-Tost, R.; Maireles-Torres, P. Gas Phase Hydrogenation of Furfural to Obtain Valuable Products Using Commercial Cr-Free Catalysts as an Environmentally Sustainable Alternative to Copper Chromite. *Journal of Environmental Chemical Engineering* **2021**, *9* (4), 105468. https://doi.org/10.1016/j.jece.2021.105468.
(30) Cao, P.; Lin, L.; Qi, H.; Chen, R.; Wu, Z.; Li, N.; Zhang, T.; Luo, W. Zeolite-Encapsulated Cu Nanoparticles for the Selective Hydrogenation of Furfural to Furfuryl Alcohol. *ACS Catal.* **2021**, 10246–10256. https://doi.org/10.1021/acscatal.1c02658.
(31) Nagaraja, B. M.; Siva Kumar, V.; Shasikala, V.; Padmasri, A. H.; Sreedhar, B.; David Raju, B.; Rama Rao, K. S. A Highly Efficient Cu/MgO Catalyst for Vapour Phase Hydrogenation of Furfural to Furfuryl Alcohol. *Catalysis Communications* **2003**, *4* (6), 287–293. https://doi.org/10.1016/S1566-7367(03)00060-8.
(32) Huang, S.; Yang, N.; Wang, S.; Sun, Y.; Zhu, Y. Tuning the Synthesis of Platinum–Copper Nanoparticles with a Hollow Core and Porous Shell for the Selective Hydrogenation of Furfural to Furfuryl Alcohol. *Nanoscale* **2016**, *8* (29), 14104–14108.
(33) Lesiak, M.; Binczarski, M.; Karski, S.; Maniukiewicz, W.; Rogowski, J.; Szubiakiewicz, E.; Berlowska, J.; Dziugan, P.; Witońska, I. Hydrogenation of Furfural over Pd–Cu/Al2O3 Catalysts. The Role of Interaction between Palladium and Copper on Determining Catalytic Properties. *Journal of Molecular Catalysis A: Chemical* **2014**, *395*, 337–348. https://doi.org/10.1016/j.molcata.2014.08.041.
(34) Wu, J.; Gao, G.; Li, J.; Sun, P.; Long, X.; Li, F. Efficient and Versatile CuNi Alloy Nanocatalysts for the Highly Selective Hydrogenation of Furfural. *Applied Catalysis B: Environmental* **2017**, *203*, 227–236.
(35) Shi, Y.; Zhu, Y.; Yang, Y.; Li, Y.-W.; Jiao, H. Exploring Furfural Catalytic Conversion on Cu(111) from Computation. *ACS Catal.* **2015**, *5* (7), 4020–4032. https://doi.org/10.1021/acscatal.5b00303.

(36) Shan, N.; Hanchett, M. K.; Liu, B. Mechanistic Insights Evaluating Ag, Pb, and Ni as Electrocatalysts for Furfural Reduction from First-Principles Methods. *J. Phys. Chem. C* **2017**, *121* (46), 25768–25777. https://doi.org/10.1021/acs.jpcc.7b06778.
(37) Zhao, Z.; Bababrik, R.; Xue, W.; Li, Y.; Briggs, N. M.; Nguyen, D.-T.; Nguyen, U.; Crossley, S. P.; Wang, S.; Wang, B.; Resasco, D. E. Solvent-Mediated Charge Separation Drives Alternative Hydrogenation Path of Furanics in Liquid Water. *Nat Catal* **2019**, *2* (5), 431–436. https://doi.org/10.1038/s41929-019-0257-z.
(38) Ren, G.; Wang, G.; Mei, H.; Xu, Y.; Huang, L. A Theoretical Insight into Furfural Conversion Catalyzed on the Ni(111) Surface. *Phys. Chem. Chem. Phys.* **2019**, *21* (42), 23685–23696. https://doi.org/10.1039/C9CP03245B.
(39) Liu, B.; Cheng, L.; Curtiss, L.; Greeley, J. Effects of van Der Waals Density Functional Corrections on Trends in Furfural Adsorption and Hydrogenation on Close-Packed Transition Metal Surfaces. *Surface Science* **2014**, *622*, 51–59. https://doi.org/10.1016/j.susc.2013.12.001.
(40) Huš, M.; Likozar, B.; Grilc, M.; others. Furfural Hydrogenation over Cu, Ni, Pd, Pt, Re, Rh and Ru Catalysts: Ab Initio Modelling of Adsorption, Desorption and Reaction Micro-Kinetics. *Chemical Engineering Journal* **2022**, *436*, 135070.
(41) Kresse, G.; Furthmüller, J. Efficient Iterative Schemes for *Ab Initio* Total-Energy Calculations Using a Plane-Wave Basis Set. *Phys. Rev. B* **1996**, *54* (16), 11169–11186. https://doi.org/10.1103/PhysRevB.54.11169.
(42) Perdew, J. P.; Burke, K.; Ernzerhof, M. Generalized Gradient Approximation Made Simple. *Physical review letters* **1996**, *77* (18), 3865.
(43) Kresse, G.; Joubert, D. From Ultrasoft Pseudopotentials to the Projector Augmented-Wave Method. *Phys. Rev. B* **1999**, *59* (3), 1758–1775. https://doi.org/10.1103/PhysRevB.59.1758.
(44) Grimme, S.; Antony, J.; Ehrlich, S.; Krieg, H. A Consistent and Accurate *Ab Initio* Parametrization of Density Functional Dispersion Correction (DFT-D) for the 94 Elements H-Pu. *The Journal of Chemical Physics* **2010**, *132* (15), 154104. https://doi.org/10.1063/1.3382344.
(45) Larsen, A. H.; Mortensen, J. J.; Blomqvist, J.; Castelli, I. E.; Christensen, R.; Du\lak, M.; Friis, J.; Groves, M. N.; Hammer, B.; Hargus, C.; others. The Atomic Simulation Environment—a Python Library for Working with Atoms. *Journal of Physics: Condensed Matter* **2017**, *29* (27), 273002.
(46) Monkhorst, H. J.; Pack, J. D. Special Points for Brillouin-Zone Integrations. *Physical review B* **1976**, *13* (12), 5188.
(47) Henkelman, G.; Uberuaga, B. P.; Jónsson, H. A Climbing Image Nudged Elastic Band Method for Finding Saddle Points and Minimum Energy Paths. *The Journal of Chemical Physics* **2000**, *113* (22), 9901–9904. https://doi.org/10.1063/1.1329672.
(48) Henkelman, G.; Jónsson, H. A Dimer Method for Finding Saddle Points on High Dimensional Potential Surfaces Using Only First Derivatives. *The Journal of Chemical Physics* **1999**, *111* (15), 7010–7022. https://doi.org/10.1063/1.480097.
(49) Medford, A. J.; Shi, C.; Hoffmann, M. J.; Lausche, A. C.; Fitzgibbon, S. R.; Bligaard, T.; Nørskov, J. K. CatMAP: A Software Package for Descriptor-Based Microkinetic Mapping of Catalytic Trends. *Catal Lett* **2015**, *145* (3), 794–807. https://doi.org/10.1007/s10562-015-1495-6.
(50) Pang, S. H.; Medlin, J. W. Adsorption and Reaction of Furfural and Furfuryl Alcohol on Pd(111): Unique Reaction Pathways for Multifunctional Reagents. *ACS Catal.* **2011**, *1* (10), 1272–1283. https://doi.org/10.1021/cs200226h.
(51) Taylor, M. J.; Jiang, L.; Reichert, J.; Papageorgiou, A. C.; Beaumont, S. K.; Wilson, K.; Lee, A. F.; Barth, J. V.; Kyriakou, G. Catalytic Hydrogenation and Hydrodeoxygenation of Furfural over Pt(111): A Model System for the Rational Design and Operation of Practical Biomass Conversion Catalysts. *J. Phys. Chem. C* **2017**, *121* (15), 8490–8497. https://doi.org/10.1021/acs.jpcc.7b01744.
(52) Wang, S.; Vorotnikov, V.; Vlachos, D. G. Coverage-Induced Conformational Effects on Activity and Selectivity: Hydrogenation and Decarbonylation of Furfural on Pd(111). *ACS Catal.* **2015**, *5* (1), 104–112. https://doi.org/10.1021/cs5015145.
(53) Shi, D.; Vohs, J. M. Deoxygenation of Biomass-Derived Oxygenates: Reaction of Furfural on Zn-Modified Pt(111). *ACS Catal.* **2015**, *5* (4), 2177–2183. https://doi.org/10.1021/acscatal.5b00038.

(54) Mironenko, A. V.; Gilkey, M. J.; Panagiotopoulou, P.; Facas, G.; Vlachos, D. G.; Xu, B. Ring Activation of Furanic Compounds on Ruthenium-Based Catalysts. *J. Phys. Chem. C* **2015**, *119* (11), 6075–6085. https://doi.org/10.1021/jp512649b.

(55) Jiménez-Gómez, C. P.; Cecilia, J. A.; García-Sancho, C.; Moreno-Tost, R.; Maireles-Torres, P. Selective Production of Furan from Gas-Phase Furfural Decarbonylation on Ni-MgO Catalysts. *ACS Sustainable Chem. Eng.* **2019**, *7* (8), 7676–7685. https://doi.org/10.1021/acssuschemeng.8b06155.

(56) Valter, M.; Santos, E. C. dos; Pettersson, L. G. M.; Hellman, A. Selectivity of the First Two Glycerol Dehydrogenation Steps Determined Using Scaling Relationships. *ACS Catal.* **2021**, 3487–3497. https://doi.org/10.1021/acscatal.0c04186.

(57) Islam, M. J.; Mesa, M. G.; Osatiashtiani, A.; Taylor, M. J.; Manayil, J. C.; Parlett, C. M.; Isaacs, M. A.; Kyriakou, G. The Effect of Metal Precursor on Copper Phase Dispersion and Nanoparticle Formation for the Catalytic Transformations of Furfural. *Applied Catalysis B: Environmental* **2020**, *273*, 119062.

(58) Weerachawanasak, P.; Krawmanee, P.; Inkamhaeng, W.; Cadete Santos Aires, F. J.; Sooknoi, T.; Panpranot, J. Development of Bimetallic Ni-Cu/SiO2 Catalysts for Liquid Phase Selective Hydrogenation of Furfural to Furfuryl Alcohol. *Catalysis Communications* **2021**, *149*, 106221. https://doi.org/10.1016/j.catcom.2020.106221.

(59) Islam, M. J.; Mesa, M. G.; Osatiashtiani, A.; Manayil, J. C.; Isaacs, M. A.; Taylor, M. J.; Tsatsos, S.; Kyriakou, G. PdCu Single Atom Alloys Supported on Alumina for the Selective Hydrogenation of Furfural. *Applied Catalysis B: Environmental* **2021**, *299*, 120652.

(60) Taylor, M. J.; Beaumont, S. K.; Islam, M. J.; Tsatsos, S.; Parlett, C. A. M.; Issacs, M. A.; Kyriakou, G. Atom Efficient PtCu Bimetallic Catalysts and Ultra Dilute Alloys for the Selective Hydrogenation of Furfural. *Applied Catalysis B: Environmental* **2021**, *284*, 119737. https://doi.org/10.1016/j.apcatb.2020.119737.

(61) Hannagan, R. T.; Giannakakis, G.; Flytzani-Stephanopoulos, M.; Sykes, E. C. H. Single-Atom Alloy Catalysis. *Chemical Reviews* **2020**, *120* (21), 12044–12088.

(62) Mao, J.; Yin, J.; Pei, J.; Wang, D.; Li, Y. Single Atom Alloy: An Emerging Atomic Site Material for Catalytic Applications. *Nano Today* **2020**, *34*, 100917.

(63) Wang, Y.; Miao, Y.; Li, S.; Gao, L.; Xiao, G. Metal-Organic Frameworks Derived Bimetallic Cu-Co Catalyst for Efficient and Selective Hydrogenation of Biomass-Derived Furfural to Furfuryl Alcohol. *Molecular Catalysis* **2017**, *436*, 128–137.

(64) Lee, J. D.; Miller, J. B.; Shneidman, A. V.; Sun, L.; Weaver, J. F.; Aizenberg, J.; Biener, J.; Boscoboinik, J. A.; Foucher, A. C.; Frenkel, A. I.; van der Hoeven, J. E. S.; Kozinsky, B.; Marcella, N.; Montemore, M. M.; Ngan, H. T.; O'Connor, C. R.; Owen, C. J.; Stacchiola, D. J.; Stach, E. A.; Madix, R. J.; Sautet, P.; Friend, C. M. Dilute Alloys Based on Au, Ag, or Cu for Efficient Catalysis: From Synthesis to Active Sites. *Chem. Rev.* **2022**, acs.chemrev.1c00967. https://doi.org/10.1021/acs.chemrev.1c00967.

(65) Liu, S.; Yang, C.; Zha, S.; Sharapa, D.; Studt, F.; Zhao, Z.; Gong, J. Moderate Surface Segregation Promotes Selective Ethanol Production in CO_2 Hydrogenation Reaction over CoCu Catalysts. *Angewandte Chemie* **2022**, *134* (2). https://doi.org/10.1002/ange.202109027.

(66) Su, Y.; Chen, C.; Zhu, X.; Zhang, Y.; Gong, W.; Zhang, H.; Zhao, H.; Wang, G. Carbon-Embedded Ni Nanocatalysts Derived from MOFs by a Sacrificial Template Method for Efficient Hydrogenation of Furfural to Tetrahydrofurfuryl Alcohol. *Dalton Transactions* **2017**, *46* (19), 6358–6365.

(67) Dong, F.; Zhu, Y.; Zheng, H.; Zhu, Y.; Li, X.; Li, Y. Cr-Free Cu-Catalysts for the Selective Hydrogenation of Biomass-Derived Furfural to 2-Methylfuran: The Synergistic Effect of Metal and Acid Sites. *Journal of Molecular Catalysis A: Chemical* **2015**, *398*, 140–148. https://doi.org/10.1016/j.molcata.2014.12.001.

(68) Byun, M. Y.; Park, D.-W.; Lee, M. S. Effect of Oxide Supports on the Activity of Pd Based Catalysts for Furfural Hydrogenation. *Catalysts* **2020**, *10* (8), 837.

(69) Tao, F. (Feng); Crozier, P. A. Atomic-Scale Observations of Catalyst Structures under Reaction Conditions and during Catalysis. *Chem. Rev.* **2016**, *116* (6), 3487–3539. https://doi.org/10.1021/cr5002657.

(70) Liu, S.; Zhao, Z.-J.; Yang, C.; Zha, S.; Neyman, K. M.; Studt, F.; Gong, J. Adsorption Preference Determines Segregation Direction: A Shortcut to More Realistic Surface Models of Alloy Catalysts. *ACS Catal.* **2019**, *9* (6), 5011–5018. https://doi.org/10.1021/acscatal.9b00499.

(71) Vogt, C.; Groeneveld, E.; Kamsma, G.; Nachtegaal, M.; Lu, L.; Kiely, C. J.; Berben, P. H.; Meirer, F.; Weckhuysen, B. M. Unravelling Structure Sensitivity in CO2 Hydrogenation over Nickel. *Nature Catalysis* **2018**, *1* (2), 127–134.